Melting experiments on komatiite analog compositions at 5 GPa

CLAUDE HERZBERG[1,2] AND JIANZHONG ZHANG[2]

[1]Department of Geological Sciences, Rutgers University, New Brunswick, New Jersey 08903, U.S.A.
[2]Center for High Pressure Research and Mineral Physics Institute, State University of New York,
Stony Brook, New York 11794, U.S.A.

ABSTRACT

The results of multi-anvil melting experiments are reported for a wide range of komatiite analog mixes with compositions in the system CaO-MgO-FeO-Fe_2O_3 ± Fe^o-Al_2O_3-SiO_2 at 5 GPa (CMAS and CMFAS ± Fe^o). The liquidus crystallization fields for olivine, orthopyroxene, clinopyroxene, and garnet were mapped out, as were their intersections at various cotectics and invariant points. For the assemblage L + Ol + Opx + Cpx + Gt, the compositions of liquids at the invariant point in CMAS and at several pseudoinvariant points in CMFAS were determined to within ±0.50 wt% (1σ). The effect of FeO is to expand the liquidus crystallization fields in the following relative ways: garnet at the expense of all other crystallizing phases, pyroxenes at the expense of olivine, and clinopyroxene at the expense of orthopyroxene. The results reported here are in excellent agreement with previous determinations (Fujii et al. 1989; Herzberg 1992; Trønnes et al. 1992), but the uncertainties are much lower. It is demonstrated that the multi-anvil apparatus is capable of yielding crystal-liquid phase-equilibrium information at 5 GPa with an accuracy that is comparable to those at lower pressures.

INTRODUCTION

Picrites and komatiites display highly variable contents of SiO_2, TiO_2, Al_2O_3, MgO, CaO, and Na_2O, which can result from variations in source-region composition, fractional crystallization, and the pressures at which the liquids formed and segregated. Of these, Al_2O_3 and the CaO/Al_2O_3 ratio are especially sensitive to the pressure at which melting and melt segregation occur, and komatiites record multiple saturation at ~ 3–10 GPa in the upper mantle (Herzberg 1992, 1995; Herzberg and Zhang 1996). And because hotter plumes melt deeper, at least for anhydrous systems, pressure information places constraints on the thermal characteristics of plumes; this is typically 100–200 °C higher than ambient mantle temperatures (Nisbet et al. 1993; Abbott et al. 1994; Herzberg 1995; Herzberg and Zhang 1996). If plumes were 400 °C hotter in the Archean Earth, they could have melted at the top of the lower mantle (Steinbach and Yuen 1994; Herzberg 1995), and this would be consistent with perovskite trace element signatures in some komatiites (Xie et al. 1993). But these trace element interpretations are presently controversial (Lahaye et al. 1995), and there are no experimental constraints on the major element geochemical identity of magmas formed at about 20 GPa. The important point is that the geochemistry of komatiites holds considerable promise for providing constraints on the scale of mass transfer in the Earth (Cawthorn 1975; Nisbet et al. 1993; Abbott et al. 1994; Herzberg 1995).

Changes in the composition of picrites and komatiites result from phase-equilibrium responses to temperature and pressure, especially the stabilization of garnet in the upper mantle and transition zone and the contraction of the liquidus olivine field. High-pressure liquidus phase diagrams are therefore very useful, and many have appeared in the 5–25 GPa pressure range from multi-anvil experiments on komatiites and peridotites (Takahashi and Scarfe 1985; Takahashi 1986; Ito and Takahashi 1987; Fujii et al. 1989; Herzberg et al. 1990; Wei et al. 1990; Herzberg 1992; Canil 1992; Trønnes et al. 1992; Zhang and Herzberg 1994; McFarlane et al. 1994; Herzberg and Zhang 1996). Constraints can be obtained on the compositions of liquids on the solidus by observing the nature of the liquidus phase for these compositions (Herzberg 1992), but there are large uncertainties because of the low *P-T-X* spatial resolution. In the 2.5–10 GPa range, the uncertainties quoted in Herzberg (1992, 1995) can propagate to ±10% uncertainties in the estimated pressure of multiple saturation; but this error may be as high as ±20%, on the basis of a comparison with liquid compositions that were independently constrained by partitioning studies (Herzberg and Zhang 1996). The 3,500 Myr Barberton komatiites have a range of CaO:Al_2O_3 that indicates multiple saturation pressures of 8–11 GPa, and added to this is a ±2 GPa experimental uncertainty (Herzberg and Zhang 1996). Given that the onset of melting must have taken place at a higher pressure than multiple saturation and eventual melt segregation, these uncertainties begin to seriously impact interpretations concerning mass transport in the upper mantle and transition zone.

The present study was designed to reduce these uncer-

tainties by examining the phase equilibria of a broad range of compositions at a single pressure, 5 GPa. Although Barberton-like komatiites appear to have formed at higher pressures, we initially focused our attention at 5 GPa as a medium pressure reference point for interpreting experiments in the 10–15 GPa range, currently in progress. From a logistical point of view, if high-resolution experiments cannot be performed at 5 GPa, then clearly useful data at higher pressures are out of the question. We report here the compositions of liquids for the equilibrium L + Ol + Opx + Cpx + Gt and for various eminating cotectics by performing experiments on many komatiite analog compositions in the system CaO-MgO-Fe^0-FeO-Fe_2O_3-Al_2O_3-SiO_2. This is a useful system to explore because it represents about 98–99% of the geochemistry of a komatiite in nature when normalized to an H_2O-free composition.

EXPERIMENTAL METHOD

Bulk compositions of all mixes used in these experiments are listed in Table 1. Compositions of mixes 18–26 are confined to the system CMAS (i.e., CaO-MgO-Al_2O_3-SiO_2) and were prepared by mixing MgO that was sintered at 1100 °C with SiO_2, Al_2O_3, and $CaCO_3$ that were oven dried at 150 °C; the mixture was then fired at 1100 °C to break down the carbonate. For mixes 1–17, Fe was introduced as oven-dried FeO to a CMAS mixture, and some of these also had 10% iron metal added to them (2, 3, 8, 13, 14, 15, and 17). Experiments were thus performed on a total of 34 mixes. Each mix was prepared as a 1 g batch, and the constituent oxides were weighed to the fourth decimal place (Table 1); uncertainties stemming from weighing are therefore negligible.

The starting materials were loaded into unwelded rhenium foil capsules and placed into an octahedral assembly with a 14 mm edge length, as described in Zhang and Herzberg (1994). In addition to the sample, the assembly contained a lanthanum chromite heater, a thermocouple (W3%Re vs. W25%Re), and spacers; this configuration was then fired at 1000 °C to expel all H_2O. The assembly was pressurized in the 2000 ton press at the High Pressure Laboratory at Stony Brook at 140 bars oil pressure, identical to the condition described before (Zhang and Herzberg 1994). About 20 min of heating was required to reach target temperature, which was 1750–1850 °C depending on the composition of the starting material. When the target temperature was reached, the experiment was allowed to run from 7 to 60 min in duration, and it was terminated by turning off the power. A 10^5 Pa thermocouple emf-temperature relation was used with no corrections made for pressure, although rough estimates place $\partial T_c/\partial P$ at about −5 °C/GPa (Zhang and Herzberg 1994).

Experimental charges were mounted in epoxy, polished, and examined with backscattered scanning electron microscopy, and wavelength-dispersive analysis of the phases was performed using the Rutgers JEOL 3600 electron microprobe. A beam current of 20 na was used with a 20 KeV accelerating voltage, and counting times ranged from 5 to 24 s to obtain standard deviations of <1% on Si, Al, Fe, Mg, and Ca. Standards used were diopside for Si and Ca, pyrope for Al, pure forsterite for Mg, and orthopyroxene for Fe. Crystalline phases were analyzed with a focused electron beam, and the liquid phase by rastering at a magnification of 2000× with calibration in the rastor mode; the area of liquid analyzed was approximately 40 × 60 μm. For both phase types, only those analyses that totaled 100 ± 1% were accepted.

Straight lanthanum chromite heaters were used in the 14 mm assemblies, and this yielded a nonlinear temperature gradient of about 20–100 °C/mm, the size of which increases with distance away from the hot spot (Zhang and Herzberg 1994). Detailed discussions of melting experiments in a temperature gradient have been previously given (Herzberg et al. 1990; Zhang and Herzberg 1994; Herzberg and Zhang 1996). Experimental charges typically have the following structure: pockets of pure liquid near the hot spot; an assemblage of crystals + liquid positioned between the solidus-liquidus melting interval; and an unmelted area at the cold end. Figure 1 shows the results of two experiments performed on mix 18, but for different durations. For both 7 min and 60 min experiments, the crystallization sequence with decreasing temperature is the same: Orthopyroxene is clearly identifiable as the liquidus phase; the second crystallizing phase is garnet with an abundance that increases with decreasing temperature; clinopyroxene is the third crystallizing phase, and olivine appears outside the field of view. The essential difference between the two experiments is textural. The 7 min experiment contains a substantial amount of intercumulus liquid between liquidus orthopyroxene, whereas the 60 min experiment does not. In experiments of long duration or elevated temperature gradient, simultaneous dissolution and precipitation of the crystalline phases accompanies a redistribution of intercumulus liquid. Similar observations were made in a time series of experiments on peridotite KLB-1 at 2135 °C and 15.5 GPa (Zhang and Herzberg 1994); longer duration experiments cause grain coarsening because of solution and precipitation, but the identity of the liquidus phase never changes. Electron microprobe analyses of the liquid pockets along the temperature gradient showed no effects of Soret diffusion in this or previous studies (Walter 1993; Herzberg and Zhang 1996). The advantages of working in a temperature gradient are immediately obvious: If the temperature interval between the liquidus and solidus is small (i.e., < ~100 °C), the crystallization sequence within the melting interval can be determined in a single experiment; solution and precipitation is a criterion for equilibrium and can promote crystalline phase homogeneity (Walker and Agee 1989; Herzberg et al. 1990; Zhang and Herzberg 1994); finally, a large pool of quench liquid can be easily analyzed with the electron microprobe, and this liquid composition is less susceptible to modification by quench crystallization in comparison with experiments containing low melt fractions. A disadvantage of working

Mix 18

$T = 1800\,°C$
$P = 5$ GPa
time = 7 minutes

$T = 1800\,°C$
$P = 5$ GPa
time = 60 minutes
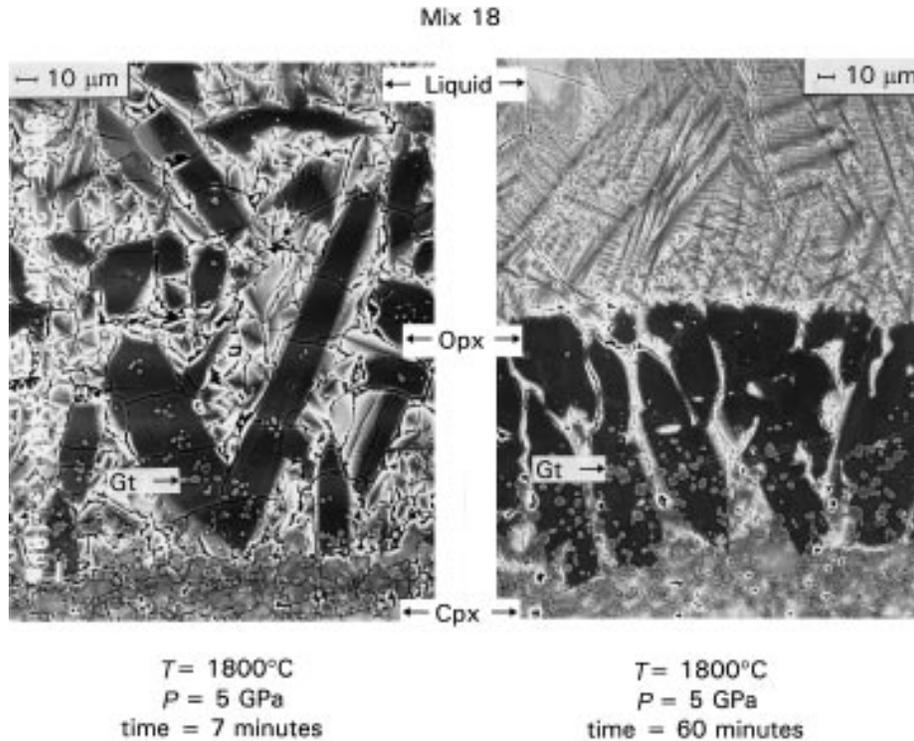
FIGURE 1. Backscattered scanning electron microscope images of experiments on mix 18. The 7 min experiment shows euhedral liquidus orthopyroxene crystals immersed in a substantial amount of quench intercumulus liquid; the 60 min experiment shows the effect of the temperature gradient in dissolving and reprecipitating the liquidus orthopyroxene into bands of anhedral crystals.

with a temperature gradient is that it can contribute to uncertainties in analyzed liquid compositions in experiments that have a substantial temperature interval between the solidus and liquidus, but the magnitude is usually no greater than the effects of quench crystallization (Herzberg and Zhang 1996).

An additional criterion for equilibrium involves use of the exchange of FeO and MgO between crystalline and liquid phases, which is quantified by the exchange coefficient

$$K_{D\,FeO/MgO}^{Xtl-L} = (FeO/MgO)_{Xtl}/(FeO/MgO)_L.$$

A time series of experiments was performed on oxide mix 15 that had 10% iron metal added, and the results are listed in Table 1 and illustrated in Figure 2. It can be seen that K_D for olivine and liquid is 0.36 ± 0.01 (1σ), and this value remains constant for experiments that range from 5 to 60 min in duration.

Rhenium was chosen as a sample container because of its high melting temperature and ease of fabrication, but it is not without problems. Figure 3 shows that the Rhenium capsules can gain up to 1% Fe within 1 μm of an Fe-bearing charge. Although this is a comparatively small amount, the loss of Fe from the sample results in an elevated O content. In the experiments reported below that were Fe free, this resulted in the creation of a small amount of Fe_2O_3, a problem discussed is more detail below.

EXPERIMENTAL RESULTS

Phase-equilibrium results for each experiment and selected electron microprobe data of quench liquid and crystalline phases are listed in Table 1. The succession of liquid + crystal assemblages observed down the temperature gradient from hot to cold is given as the crystallization sequence (see above). The temperatures listed are those recorded by the thermocouple and are within about $\pm 50\,°C$ of the liquidus temperatures of the starting materials. The results are shown in Figures 4 and 5.

The compositions of the mixed oxide starting materials in both CMAS and CMFAS are shown together with their liquidus crystallization fields in Figures 4a and 4b and 5a and 5b. Most oxide compositions are contained within the garnet peridotite tetrahedron Ol-En-Di-Gt, and Figure 4 is one view from diopside into the plane olivine–enstatite–magnesium Tschermak's. This particular plane was chosen because it includes liquids for the cotectic equilibrium L + Ol + Di + Gt, many of which plot on the En-poor side of the plane Ol-Di-Gt. Figure 5 is a projection from enstatite into the plane Ol-Gt-Di.

The peritectic point involving L + Fo + Opx + Di + Gt in CMAS was tightly bracketed by mixes 21, 25, and 24 (Figs. 4a and 5a). Photomicrographs of these experiments in Figure 6 show how sensitive the liquidus phase mineralogy is to small changes in bulk composition near a multiple saturation point. The liquid at this peritectic

TABLE 1. Experimental results (wt%) at 5 GPa

Mix	T (°C)	t (min)	Crystallization sequence	Phase	No. of analyses	SiO_2	Al_2O_3	FeO	MgO	CaO	Total	K_D Xtl/L
1	1750	7		Mix		46.39	9.02	11.04	24.55	9.02	100.00	
			L	L	49	46.11(0.26)	8.61(0.09)	12.24(0.20)	23.63(0.22)	9.49(0.15)	100.20	
			L + Gt	Gt	55	43.15(0.43)	23.21(0.42)	6.43(0.56)	22.17(0.82)	5.43(0.80)	100.55	0.56(0.06)
			L + Gt + Ol	Ol	20	41.04(0.30)	0.27(0.07)	8.55(0.14)	50.31(0.37)	0.38(0.02)	100.55	0.33(0.01)
			L + Gt + Ol + Cpx	Cpx	19	55.27(0.53)	3.52(0.62)	5.39(0.26)	28.57(1.01)	7.46(0.90)	100.24	0.36(0.02)
2	1850	5		Mix		48.08	4.78	10.83	31.85	4.46	100.00	
			L	L	42	48.27(0.09)	5.28(0.13)	12.40(0.12)	29.21(0.57)	5.10(0.12)	100.26	
			L + Ol	Ol	18	41.22(0.19)	0.15(0.01)	7.77(0.17)	50.21(0.23)	0.19(0.01)	99.54	0.37(0.01)
			L + Ol + Opx									
2 + 10% Fe°	1850	5	L	L	36	46.58(0.89)	4.80(0.38)	15.80(0.49)	28.40(1.36)	4.52(0.31)	100.10	
			L + Ol + Fe°	Ol	21	40.58(0.22)	0.12(0.01)	10.21(0.15)	48.46(0.24)	0.17(0.01)	99.54	0.38(0.02)
			L + Ol + Opx + Fe°									
3	1850	8		Mix		48.89	5.31	10.91	29.94	4.96	100.00	
			L	L	23	48.51(0.27)	5.44(0.08)	11.74(0.19)	28.86(0.25)	5.76(0.11)	100.30	
			L + Ol	Ol	24	40.68(0.27)	0.15(0.04)	8.15(0.20)	51.29(0.45)	0.22(0.01)	100.49	0.39(0.01)
			L + Ol + Opx									
3 + 10% Fe°	1850	6	L	L	50	47.40(0.34)	5.56(0.13)	15.27(0.34)	26.46(0.26)	5.32(0.12)	100.01	
			L + Ol + Opx + Fe°	Ol	24	40.30(0.37)	0.14(0.01)	10.12(0.13)	49.06(0.36)	0.20(0.02)	99.82	0.36(0.01)
				Opx	17	55.71(0.67)	2.09(0.40)	6.32(0.41)	33.85(0.67)	1.72(0.29)	99.69	0.32(0.02)
4	1750	11	L	Mix		47.41	8.85	10.83	24.08	8.85	100.00	
			L + Opx									
			L + Opx + Gt									
5	1750	6	L	Mix		48.39	8.68	10.63	23.63	8.68	100.00	
			L + Opx									
			L + Opx + Gt									
			L + Opx + Gt + Cpx									
6	1800	7	L	Mix		47.39	8.62	10.54	23.45	10.02	100.00	
			L + Cpx									
			L + Cpx + Gt									
			L + Cpx + Gt + Ol									
7	1850	7	L	Mix		49.27	5.56	10.90	29.08	5.19	100.00	
			L + Opx									
			L + Opx + Ol									
8	1750	6	L	Mix		46.90	8.68	10.90	24.30	9.22	100.00	
			L + Gt									
			L + Gt + Cpx									
			L + Gt + Cpx + Ol									
8 + 10% Fe°	1800	7	L	L	57	46.10(0.46)	8.31(0.13)	12.79(0.43)	23.60(0.27)	9.22(0.14)	100.03	
			L + Ol + Fe°	Ol	12	40.39(0.30)	0.20(0.01)	10.03(0.12)	49.37(0.29)	0.39(0.05)	100.38	0.37(0.02)
			L + Ol + Gt + Fe°									
			L + Ol + Gt + Cpx + Fe°									
9	1800	6	L	Mix		47.20	8.68	10.90	24.00	9.22	100.00	
			L + Gt									
			L + Gt + Cpx									
			L + Gt + Cpx + Ol									
10	1800	6		Mix		46.80	8.56	11.04	24.86	8.76	100.00	
			L	L	121	46.31(0.48)	8.65(0.11)	11.71(0.47)	24.16(0.32)	9.21(0.24)	100.04	
			L + Opx1	Opx1	12	55.54(0.40)	3.78(0.23)	5.22(0.10)	33.11(0.31)	2.59(0.20)	100.24	0.33(0.02)
			L + Opx2 + Ol2	Opx2	9	55.29(0.28)	3.92(0.46)	5.36(0.09)	32.94(0.22)	2.80(0.15)	100.31	
			L + Ol + Gt	Ol2	10	40.55(0.38)	0.22(0.02)	9.02(0.16)	50.52(0.36)	0.35(0.06)	100.66	
			L + Ol + Gt + Cpx									
11	1750	7	L + Ol + Gt + Cpx (Opx near hot spot)	Mix		47.22	8.20	11.04	25.16	8.40	100.00	
12	1750	6	L	Mix		45.37	9.76	11.04	23.83	10.00	100.00	
			L + Gt									
			L + Gt + Cpx									
			L + Gt + Cpx + Ol									

TABLE 1.—*Continued*

Mix	T (°C)	t (min)	Crystallization sequence	Phase	No. of analyses	SiO$_2$	Al$_2$O$_3$	FeO	MgO	CaO	Total	K_D Xtl/L
13	1800	6		Mix		46.66	8.68	11.04	24.76	8.88	100.00	
			L	L	30	47.34(0.32)	8.55(0.09)	11.54(0.29)	23.67(0.21)	9.10(0.14)	100.20	
			L + Opx	Opx	15	56.22(0.30)	3.49(0.39)	4.91(0.08)	32.97(0.36)	2.77(0.20)	100.36	0.31(0.01)
			L + Opx + Gt	Gt	23	43.11(0.49)	23.13(0.33)	6.02(0.42)	22.93(0.55)	4.70(0.31)	99.89	0.54(0.04)
			L + Gt + Cpx	Cpx	14	55.45(0.36)	3.11(0.14)	5.42(0.14)	29.33(0.55)	7.05(0.61)	100.18	0.36(0.02)
			L + Gt + Cpx + Ol									
13+ 10% Fe°	1800	7	L	L	56	45.93(0.20)	8.44(0.09)	14.89(0.20)	22.27(0.15)	8.59(0.09)	100.12	
			L + Opx	Opx	26	55.56(0.38)	3.51(0.53)	6.78(0.19)	31.70(0.42)	2.53(0.20)	100.08	0.32(0.01)
			L + Ol + Gt	Ol	22	40.66(0.26)	0.20(0.01)	11.62(0.22)	47.59(0.21)	0.33(0.02)	100.40	0.36(0.01)
			L + Ol + Gt	Gt	28	43.52(0.43)	23.54(0.49)	7.15(0.42)	22.15(0.65)	4.42(0.33)	100.78	0.48(0.03)
			+ Cpx	Cpx	26	55.22(0.52)	3.23(0.36)	7.18(0.30)	28.41(1.00)	6.27(1.04)	100.31	0.38(0.02)
14	1800	5		Mix		46.59	8.57	11.04	24.70	9.10	100.00	
			L	L	47	46.42(0.32)	8.58(0.11)	11.47(0.27)	24.19(0.18)	9.29(0.13)	99.95	
			L + Opx	Opx	23	56.60(0.55)	3.58(0.56)	4.59(0.08)	33.13(0.44)	2.63(0.12)	100.53	0.29(0.01)
			L + Opx + Gt	Gt	8	43.70(0.65)	23.44(0.39)	5.28(1.12)	23.60(1.29)	4.40(0.79)	100.42	0.47(0.10)
			L + Ol + Gt	Ol	9	41.58(0.35)	0.46(0.25)	7.55(0.11)	50.48(0.34)	0.39(0.05)	100.46	0.32(0.01)
			+ Cpx	Cpx	14	54.99(0.54)	3.47(0.18)	4.95(0.11)	28.66(0.63)	7.81(0.72)	99.88	0.36(0.01)
14 + 10% Fe°	1800	7	L	L	39	45.06(0.17)	8.10(0.16)	17.06(0.22)	21.87(0.27)	8.03(0.10)	100.12	
			L + Ol	Ol	21	40.08(0.27)	0.20(0.01)	12.73(0.17)	47.18(0.19)	0.33(0.01)	100.52	0.35(0.01)
			L + Ol + Gt	Gt	23	43.14(0.59)	22.88(0.37)	8.18(1.19)	22.31(1.76)	4.27(1.59)	100.78	0.47(0.08)
			L + Ol + Gt	Cpx	16	54.42(0.37)	3.04(0.19)	7.89(0.26)	27.32(0.78)	7.53(0.88)	100.20	0.37(0.02)
			+ Cpx									
14 + 10% Fe° + CaO	1750	7	L	L	15	43.78(0.23)	7.71(0.12)	18.11(0.12)	21.30(0.26)	9.45(0.16)	100.35	
			L + Ol									
			L + Ol + Gt									
15	1800	7		Mix		46.40	8.40	11.04	24.86	9.30	100.00	
			L	L	80	46.19(0.25)	8.32(0.08)	12.33(0.23)	23.52(0.18)	9.77(0.12)	100.13	
			L + Opx	Opx	8	55.86(0.30)	3.06(0.27)	5.10(0.24)	33.00(0.48)	3.01(0.39)	100.03	0.29(0.01)
			L + Ol + Cpx	Ol	32	40.69(0.23)	0.27(0.09)	8.46(0.25)	50.15(0.39)	0.40(0.05)	99.97	0.32(0.01)
			L + Ol + Cpx	Cpx	27	54.49(0.33)	3.68(0.16)	5.18(0.09)	28.43(0.59)	8.03(0.60)	99.82	0.35(0.01)
			+Gt	Gt	29	42.86(0.51)	23.53(0.46)	6.32(0.81)	21.99(0.92)	5.40(0.55)	100.10	0.55(0.08)
15 + 10% Fe°	1800	5	L	L	40	44.31(0.23)	8.09(0.10)	17.33(0.26)	21.22(0.21)	9.25(0.11)	100.20	
			L + Ol	Ol	18	40.58(0.42)	0.18(0.01)	13.09(0.40)	45.50(0.34)	0.39(0.02)	99.74	0.36(0.01)
			L + Ol + Gt									
			L + Ol + Gt									
			+ Cpx									
15 + 10% Fe°	1800	15	L	L	48	45.07(0.28)	8.01(0.17)	16.51(0.33)	22.18(0.19)	9.06(0.18)	100.82	
			L + Ol	Ol	22	39.95(0.24)	0.20(0.01)	12.56(0.12)	47.29(0.40)	0.37(0.01)	100.37	0.36(0.01)
			L + Ol + Gt									
			L + Ol + Gt									
			+ Cpx									
15 + 10% Fe°	1800	60	L	L	41	45.02(0.42)	8.45(0.10)	17.67(0.26)	19.96(0.19)	9.45(0.12)	100.55	
			L + Ol	Ol	16	40.29(0.24)	0.19(0.01)	14.16(0.17)	45.55(0.27)	0.36(0.01)	100.55	0.35(0.01)
			L + Ol + Gt									
			L + Ol + Gt									
			+ Cpx									
15 + 20% Fe°	1800	5	L	L	30	44.05(0.54)	7.78(0.12)	18.18(0.26)	22.27(0.29)	8.51(0.13)	100.78	
			L + Ol	Ol	16	39.66(0.20)	0.20(0.01)	13.52(0.17)	46.69(0.22)	0.38(0.02)	100.44	0.35(0.01)
			L + Ol + Gt									
			L + Ol + Gt									
			+ Cpx									
16	1800	7		Mix		46.20	8.20	11.04	25.06	9.50	100.00	
			L	L	34	46.35(0.27)	8.27(0.11)	11.56(0.22)	24.02(0.16)	9.76(0.10)	99.97	
			L + Ol	Ol	15	41.18(0.23)	0.24(0.06)	7.71(0.18)	50.75(0.21)	0.40(0.06)	100.28	0.32(0.01)
			L + Ol + Cpx									
			L + Ol + Cpx									
			+ Gt									
17	1800	7		Mix		46.40	8.60	11.04	24.46	9.50	100.00	
			L	L	50	46.09(0.24)	8.45(0.10)	12.65(0.22)	22.88(0.19)	10.01(0.13)	100.08	
			L + Opx	Opx	17	55.47(0.21)	3.59(0.26)	5.38(0.17)	32.91(0.20)	2.99(0.21)	100.34	0.30(0.01)
			L + Cpx	Cpx	16	54.54(0.23)	3.48(0.26)	5.29(0.10)	28.28(0.55)	8.22(0.68)	99.81	0.34(0.01)
			L + Cpx + Ol	Ol	16	40.73(0.24)	0.35(0.16)	8.68(0.16)	50.16(0.25)	0.39(0.03)	100.31	0.32(0.01)
			+ Gt	Gt	20	43.15(0.44)	23.63(0.29)	6.31(0.51)	22.75(0.83)	5.23(0.66)	101.07	0.51(0.05)
17 + 10% Fe°	1800	7	L	L	36	45.00(0.29)	7.83(0.10)	16.16(0.28)	22.24(0.09)	8.54(0.11)	99.77	
			L + Ol	Ol	23	39.90(0.22)	0.21(0.04)	12.62(0.15)	46.81(0.23)	0.36(0.02)	99.90	0.37(0.01)
			L + Ol + Gt	Gt	30	43.19(0.75)	23.48(0.75)	7.74(0.86)	21.52(1.55)	4.43(1.12)	100.36	0.49(0.06)
			L + Ol + Gt	Cpx	16	54.27(0.30)	2.98(0.16)	7.46(0.13)	26.60(0.64)	8.28(0.79)	99.59	0.38(0.01)
			+ Cpx									

TABLE 1.—*Continued*

Mix	T (°C)	t (min)	Crystallization sequence	Phase	No. of analyses	SiO₂	Al₂O₃	FeO	MgO	CaO	Total	K_D Xtl/L
18	1800	7	L	Mix		49.50	10.00	0	30.50	10.00	100.00	
			L + Opx									
			L + Opx + Gt									
			L + Opx + Gt									
			+ Cpx									
18	1800	60	L	Mix		49.50	10.00	0	30.50	10.00	100.00	
			L + Opx									
			L + Opx + Gt									
			L + Opx + Gt									
			+ Cpx									
19	1800	7	L	Mix		50.50	10.00	0	29.50	10.00	100.00	
			L + Opx									
			L + Opx + Gt									
			L + Opx + Gt									
			+ Cpx									
20	1800	7	L	Mix		50.50	9.00	0	29.50	11.00	100.00	
			L + Opx									
			L + Opx + Cpx									
			L + Opx + Cpx									
			+ Gt									
21	1800	7	L	Mix		48.50	10.00	0	31.50	10.00	100.00	
			L + Ol									
			L + Ol + Gt									
			L + Ol + Gt									
			+ Cpx									
22	1800	7		Mix		47.50	10.00	0	32.50	10.00	100.00	
			L	L	10	47.52(0.39)	9.69(0.24)	0	32.11(0.95)	9.79(0.22)	99.11	
			L + Ol									
			L + Ol + Gt									
			L + Ol + Gt									
			+ Cpx									
23	1800	7		Mix		47.00	9.50	0	34.00	9.50	100.00	
			L	L	13	47.67(0.46)	9.92(0.55)	0	33.26(1.82)	9.68(0.70)	100.53	
			L + Ol									
			L + Ol + Gt									
			L + Ol + Gt									
			+ Cpx									
24	1800	7	L	Mix		49.00	9.60	0	31.00	10.40	100.00	
			L + Opx	Opx	24	57.26(0.36)	3.54(0.45)	0	35.88(0.39)	3.01(0.25)	99.57	
			L + Opx + Gt	Gt	17	44.31(0.30)	24.79(0.21)	0	25.60(0.41)	5.47(0.42)	100.17	
			L + Opx + Gt	Cpx	24	56.00(0.34)	3.37(0.27)	0	30.22(0.95)	10.03(1.10)	99.62	
			+ Cpx + Ol	Ol	3	42.66(0.17)	0.20(0.01)	0	56.37(0.32)	0.34(0.02)	99.57	
24	1800	60	L	Mix		49.00	9.60	0	31.00	10.40	100.00	
			L + Opx									
			L + Opx + Ol									
			L + Opx + Ol									
			+ Gt									
			L + Opx + Ol									
			+ Gt + Cpx									
25	1780	7		Mix		49.00	9.30	0	31.00	10.70	100.00	
			L	L	9	49.11(0.38)	8.71(0.20)	0	31.02(0.44)	10.43(0.31)	99.27	
			L + Ol + Opx	Ol	6	42.43(0.39)	0.21(0.01)	0	57.02(0.19)	0.31(0.01)	99.96	
			+ Cpx	Opx	11	57.14(0.34)	3.61(0.39)	0	36.19(0.21)	3.12(0.10)	100.06	
			L + Ol + Opx	Cpx	34	55.60(0.55)	4.19(0.67)	0	31.02(0.88)	8.94(0.85)	99.75	
			+ Cpx + Gt	Gt	32	43.90(0.30)	24.41(0.39)	0	25.81(0.47)	5.70(0.53)	99.82	
				Q Cpx	6	52.30(0.69)	8.56(0.42)	0	28.70(1.09)	10.01(1.01)	99.58	
26	1800	7	L	Mix		52.18	9.02	0	28.22	10.89	100.31	
			L + Opx									
			L + Opx + Cpx									

Notes: Mix = oxide mix, L = liquid, Ol = olivine, Opx = orthopyroxene, Cpx = clinopyroxene, Q Cpx = quench clinopyroxene, Gt = garnet. K_D Xtl/L = (FeO/MgO)_{Xtl}/(FeO/MgO)_L. Numbers in parentheses equal 1σ.

point has the following composition: SiO₂ = 48.85(0.18), Al₂O₃ = 9.55(0.13), MgO = 30.90(0.30), and CaO = 10.70(0.15) wt%, with small uncertainties (1σ) resulting from the small spread of compositions used to bracket the liquid.

Electron microprobe compositions of some quench liq-uids are included in Table 1. Where good probe analyses were possible, there is good agreement with the bulk composition. However, liquid analyses with 100 ± 1% totals could be obtained only for the more MgO-rich sam-ples, a problem that results from compositional depen-dence on the liquid quench textures. Liquids with higher
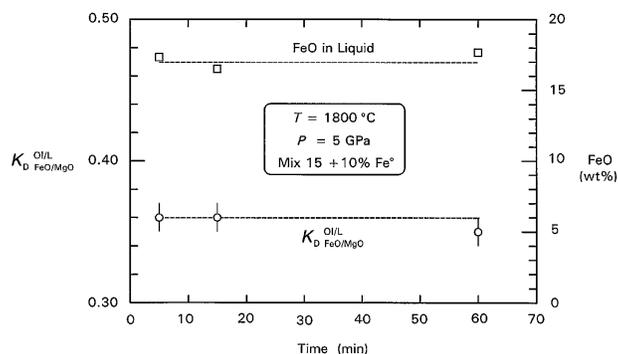
**FIGURE 2.** Time series experiments on mix 15 + 10% Fe[0] metal. Olivine is the liquidus phase in all cases (Table 1).

FIGURE 3. Fe content of rhenium capsule as a function of distance away from the sample, which is mix 15 without metallic Fe.

contents of SiO_2 quench to a complex intergrowth of small quench olivine crystals imbedded in large quench clinopyroxene crystals, some of which can be seen in Figure 6. Many of the small quench olivine crystals were unavoidably plucked during polishing, resulting in a surface that was highly porous, the cause of the low totals; epoxy impregnation did not help because the pore spaces were found to be unconnected. The quench clinopyroxene crystals are variable in composition, but representative analyses are included in Table 1 for mix 25. As discussed below, addition of FeO to CMAS lowers the size of the quench crystals and results in good electron probe analyses.

Inspection of Figures 4 and 5 shows that our new peritectic liquid composition for the equilibrium L + Ol + Opx + Cpx + Gt in CMAS agrees very well with the estimates given by Herzberg (1992) and Fujii et al. (1989). We tested the Herzberg (1992) estimate by preparing and heating mix 18; Figure 1 shows that mix 18 is not multiply saturated in Ol + Opx + Cpx + Gt, but rather it is saturated in orthopyroxene only. Although the composition of mix 18 is very similar to our new and preferred peritectic liquid composition, the small differences are clearly resolvable.

For oxide mixes with approximately 11 wt% FeO in CMFAS, the pseudoinvariant point involving L + Ol + Opx + Cpx + Gt was also tightly bracketed by mixes 1 and 13–17 (Figs. 4b and 5b), and its composition is listed in Table 2. The identity of the liquidus phase is so sensitive to the bulk oxide composition near invariant points and cotectics that we were able to resolve a slight curvature to the cotectic L + Opx + Cpx + Gt. The liquid composition at the invariant point is SiO_2 = 46.30(0.30), Al_2O_3 = 8.65(0.25), FeO = 11.04, MgO = 24.67(0.20), and CaO = 9.34(0.30) wt%. Error bars result from the spread of compositions of the mixes used to bracket the liquid (1σ), and contributions from uncertainties in weighing the oxides are negligible.

Electron microprobe analyses of quench liquids in CMFAS are also reported in Table 1 and were found to be less susceptible to quench problems than liquids quenched in CMAS. Inspection of this table demonstrates
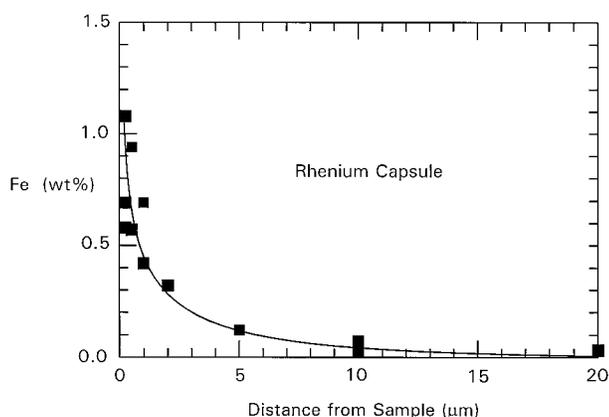
that liquids analyzed by the electron probe are very similar to the bulk compositions of the oxide mixes, except they are modestly enriched in Fe and depleted in MgO and SiO_2. This difference arises from the migration of liquid from the cold to the hot directions of the temperature gradient. Electron probe data have total Fe reported as FeO, and the liquid composition at the pseudoinvariant point is (Table 2) SiO_2 = 46.06(0.55), Al_2O_3 = 8.40(0.25), FeO = 12.20(0.50), MgO = 23.60(0.50), and CaO = 9.74(0.30) wt%. Error bars (1σ) are the sum of uncertainties from the electron probe analyses and the compositions of the mixes used to bracket the liquid.

Some Fe was lost from the CMFAS oxide mixes to the rhenium capsules, and the amount is shown in Figure 3. The capsules changed from being essentially pure Fe to containing 0.5–1.0 wt% Fe within 1 μm of the contact with the samples. Because all Fe was essentially FeO in the starting material, this resulted in a surplus of O in the samples and oxidation of some of the original FeO to Fe_2O_3. The amount of Fe_2O_3 can be roughly estimated by examining the experiments in CMFAS that had 10 wt% Fe[0] metal included.

For experiments in CMFAS + Fe[0], the metal appeared as rounded and melted droplets that were trapped within a matrix of crystals ± silicate liquid. Electron probe analyses showed the droplets to be essentially pure Fe throughout most of the charge, but those next to the rhenium capsule wall contained about 0.6% Re. In the hottest portions of the charges, where there existed pockets of total melt, iron metal was absent because of gravity settling onto the rhenium container, and this resulted in ~5 μm Re-Fe alloy rims on the container with 18–33 wt% Fe. For the silicate crystalline and liquid phases coexisting with iron metal, it is reasonable to assume that all the Fe measured in the probe analyses was FeO, making it possible to evaluate with some confidence the exchange coefficient K_D. From Table 1, the following averages were obtained for experiments in CMFAS + Fe[0]: $K_{D\ FeO/MgO}^{Ol/L}$ = 0.36(0.02), $K_{D\ FeO/MgO}^{Opx/L}$ = 0.32(0.02), $K_{D\ FeO/MgO}^{Cpx/L}$ = 0.38(0.02), $K_{D\ FeO/MgO}^{Gt/L}$ = 0.48(0.06), with uncertainties at the 1σ level.

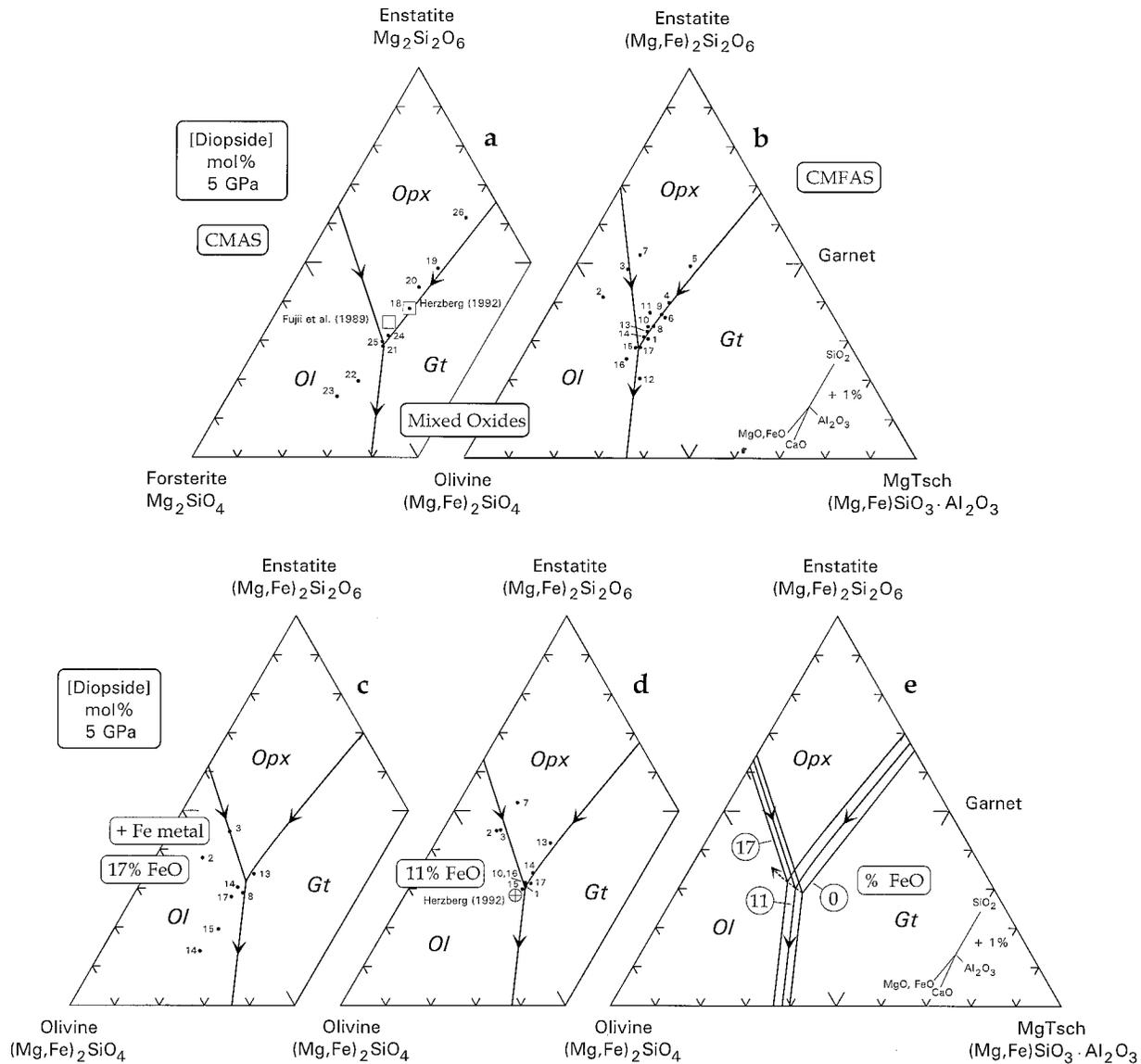**FIGURE 4.** Projection of compositions and liquidus phase boundaries from diopside ($CaMgSi_2O_6$) into the plane olivine–enstatite–magnesium Tschermak's. (**a**) Oxide mixes in CMAS; (**b**) oxide mixes in CMFAS; (**c**) electron probe analyses of liquids in CMFAS + Fe[0], with liquid analyses averaging 17% FeO; (**d**) electron probe analyses of liquids in CMFAS without Fe[0], with liquid analyses averaging 11% FeO; (**e**) summary of phase boundaries showing the effects of variable FeO (wt%); inset in **e** shows how the invariant points are shifted in reponse to adding 1 wt% of the various oxides. Numbered points refer to starting material compositions given in Table 1.

Figure 2 shows that the exchange coefficient for olivine and liquid remains constant for experiment durations from 5 to 60 min, demonstrating that equilibrium is rapidly established near 1800 °C. However, garnet is sometimes zoned, and this is reflected in the larger uncertainty for $K_{D\text{FeO/MgO}}^{Gt/L}$.

Exchange coefficients were also calculated for CMFAS experiments that were Fe[0] free, and with the assumption that there was no Fe_2O_3 in any phase. The results, included in Table 1, show that K_D values for Ol/L, Opx/L, and Cpx/L are usually lower than exchange coefficients

in CMFAS + Fe[0], and K_D for Gt/L is higher. These differences point to significant amounts of Fe_2O_3 that were generated in the sample during Fe[0] loss to the rhenium capsule. An estimate can be made of the Fe_2O_3 content of liquids from the total Fe content of the liquid and from FeO constrained by $K_{D\text{FeO/MgO}}^{Ol/L} = 0.36$; we assume that the amount of Fe_2O_3 in olivine is negligible. And with the content of FeO in the liquid thus estimated, the contents of FeO and Fe_2O_3 in orthopyroxene, clinopyroxene, and garnet can also be determined from their exchange coefficients. The results of these calculations are listed in
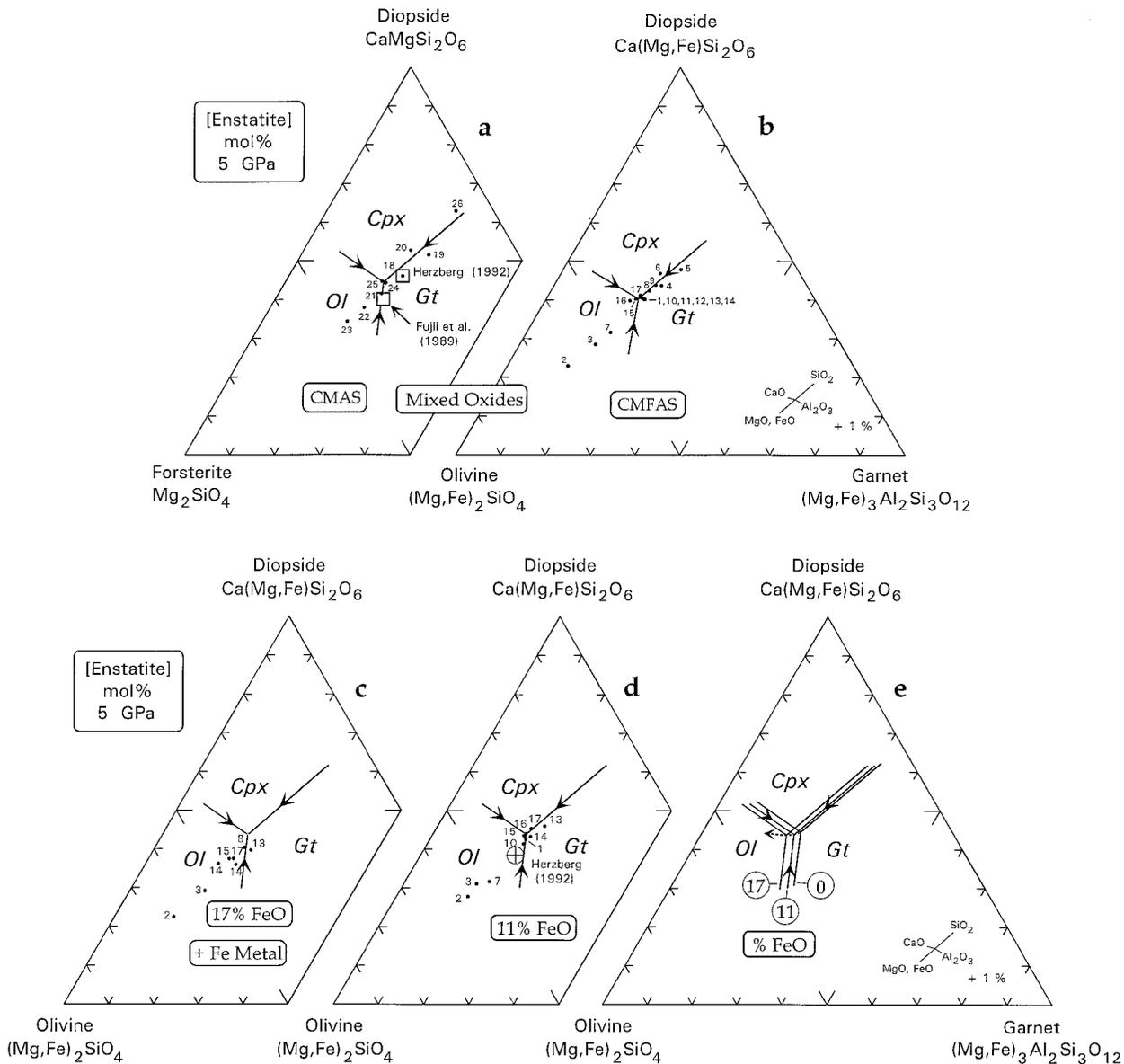
FIGURE 5. Projection of compositions and liquidus phase boundaries from enstatite ($Mg_2Si_2O_6$) into the plane olivine–diopside–garnet. (**a**) Oxide mixes in CMAS; (**b**) oxide mixes in CMFAS; (**c**) electron probe analyses of liquids in CMFAS + Fe^o, with liquid analyses averaging 17% FeO; (**d**) electron probe analyses of liquids in CMFAS without Fe^o, with liquid analyses averaging 11% FeO; (**e**) summary of phase boundaries showing the effects of variable FeO (wt%); inset in **e** shows how the invariant points are shifted in reponse to adding 1 wt% of the various oxides. Numbered points refer to starting material compositions given in Table 1.

Table 2. In all cases, the absolute weight percent of Fe_2O_3 is low, but the percentage of Fe_2O_3 to total Fe can be substantial, averaging about 13% for liquid, 20% for garnet, 4% for orthopyroxene, and 5% for clinopyroxene. Garnet contains the largest fraction of Fe as Fe_2O_3, and this results in a high K_D if its concentration is assumed to be zero. The liquid at the pseudoinvariant point in Fe-free CMFAS experiments is thus estimated to contain about 1.60% Fe_2O_3 and 10.76% FeO (Table 2).

The compositions of the liquids at the pseudoinvariant point L + Ol + Opx + Cpx + Gt for a range of possible contents of Fe_2O_3 are listed in Table 2 and shown in Figure 7. If all Fe is assumed to be FeO, the invariant point L Invpt 1 in Table 2 projects to point 1 in Figure 7. If 1.60% Fe_2O_3 is considered as L Invpt 2 in Table 2, Fe_2O_3 is added to Al_2O_3, resulting in a shift toward garnet (i.e., point 2). This makes no sense from a phase-equilibrium perspective because the effect of Fe_2O_3 should be to expand the garnet liquidus crystallization field rather than contract it. If Fe_2O_3 is treated as a neutral component by normalizing the liquids in Table 2 to Fe_2O_3-free compositions (ie., Invpt 3; Table 2), the point shifts away from
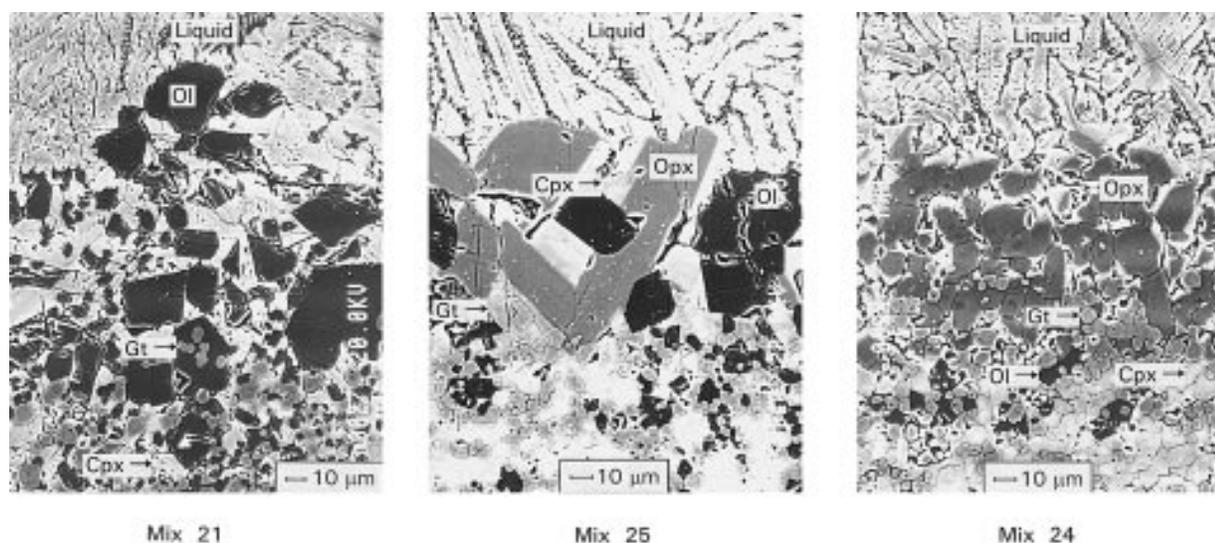
FIGURE 6. Backscattered scanning electron microscope images of experiments on mixes 21, 24, and 25 in CMAS. Note the substantial reponse in the liquidus phase mineralogy to small changes in bulk composition near an invariant point.

TABLE 2. Inferred Fe^{2+} and Fe^{3+} contents in metal-free experiments (wt%)

Mix	Phase	SiO_2	Al_2O_3	Fe_2O_3	FeO	MgO	CaO	Total
Oxide mixes	L Invpt	46.30(0.30)	8.65(0.25)	0	11.04	24.67(0.20)	9.34(0.30)	100.00
Probed liquids 1	L Invpt 1	46.06(0.55)	8.40(0.25)	0	12.20(0.50)	23.60(0.50)	9.74(0.30)	100.00
1	Mix	46.39	9.02	0	11.04	24.55	9.02	100.00
	L	46.11(0.26)	8.61(0.09)	1.20	11.16	23.63(0.22)	9.49(0.15)	100.20
	Ol	41.04(0.30)	0.27(0.07)	0	8.55(0.14)	50.31(0.37)	0.38(0.02)	100.55
	Gt	43.15(0.43)	23.21(0.42)	1.56	5.03	22.17(0.82)	5.43(0.80)	100.55
	Cpx	55.27(0.53)	3.52(0.62)	0.29	5.13	28.57(1.01)	7.46(0.90)	100.24
10	Mix	46.8	8.56	0	11.04	24.86	8.76	100.00
	L	46.31(0.48)	8.65(0.11)	0.19	11.54	24.16(0.32)	9.21(0.24)	100.06
	Opx 1	55.54(0.40)	3.78(0.23)	0.18	5.06	33.11(0.31)	2.59(0.20)	100.26
	Ol 2	40.55(0.38)	0.22(0.02)	0	9.02(0.16)	50.52(0.36)	0.35(0.06)	100.66
	Opx 2	55.29(0.28)	3.92(0.46)	0.14	5.23	32.94(0.22)	2.8 (0.15)	100.32
13	Mix	46.66	8.68	0	11.04	24.76	8.88	100.00
	L	47.34(0.32)	8.55(0.09)	1.21	10.45	23.67(0.21)	9.10(0.14)	100.32
	Opx	56.22(0.30)	3.49(0.39)	0.25	4.66	32.97(0.36)	2.77(0.20)	100.36
	Gt	43.11(0.49)	23.13(0.33)	1.29	4.86	22.93(0.55)	4.70(0.31)	100.02
	Cpx	55.45(0.36)	3.11(0.14)	0.36	4.92	29.33(0.55)	7.05(0.61)	100.22
14	Mix	46.59	8.57	0	11.04	24.70	9.10	100.00
	L	46.42(0.32)	8.58(0.11)	1.58	10.05	24.19(0.18)	9.29(0.13)	100.11
	Opx	56.6 (0.55)	3.58(0.56)	0.21	4.4	33.13(0.44)	2.63(0.12)	100.55
	Ol	41.58(0.35)	0.46(0.25)	0	7.55(0.11)	50.48(0.34)	0.39(0.05)	100.46
	Gt	43.70(0.65)	23.44(0.39)	0.63	4.71	23.60(1.29)	4.40(0.79)	100.48
	Cpx	54.99(0.54)	3.47(0.18)	0.48	4.52	28.66(0.63)	7.81(0.72)	99.93
15	Mix	46.40	8.40	0	11.04	24.86	9.30	100.00
	L	46.16(0.25)	8.32(0.08)	1.46	11.02	23.52(0.18)	9.77(0.12)	100.10
	Opx	55.86(0.30)	3.06(0.27)	0.17	4.95	33.00(0.48)	3.01(0.39)	100.05
	Ol	40.69(0.23)	0.27(0.09)	0	8.46(0.25)	50.15(0.39)	0.40(0.05)	99.97
	Gt	42.86(0.51)	23.53(0.46)	1.37	4.95	21.99(0.92)	5.40(0.55)	100.1
	Cpx	54.49(0.30)	3.68(0.06)	0.13	5.06	28.43(0.17)	8.03(0.13)	99.82
17	Mix	46.40	8.60	0	11.04	24.46	9.50	100.00
	L	46.09(0.24)	8.45(0.10)	1.83	11.00	22.88(0.19)	10.01(0.13)	100.26
	Opx	55.47(0.21)	3.59(0.26)	0.36	5.06	32.91(0.20)	2.99(0.21)	100.38
	Ol	40.73(0.24)	0.35(0.16)	0	8.68(0.16)	50.16(0.25)	0.39(0.03)	100.31
	Gt	43.15(0.44)	23.63(0.29)	1.18	5.25	22.75(0.83)	5.23(0.66)	101.19
	Cpx	54.54(0.23)	3.48(0.26)	0.13	5.17	28.28(0.55)	8.22(0.68)	99.82
Probed liquids 2	L Invpt 2	46.06(0.55)	8.40(0.25)	1.60	10.76(0.50)	23.60(0.50)	9.74(0.30)	100.16
Probed liquids 3	L Invpt 3	46.65(0.55)	8.55(0.25)	0	11.25(0.50)	23.60(0.50)	9.95(0.30)	100.00

Notes: Mix = oxide mix, L = liquid, Ol = olivine, Opx = orthopyroxene, Cpx = clinopyroxene, Gt = garnet. L Invpt = liquid at invariant point. L Invpt1, L Invpt2, and L Invpt3 = points 1, 2, and 3, respectively, in Figure 7. Numbers in parentheses equal 1σ.
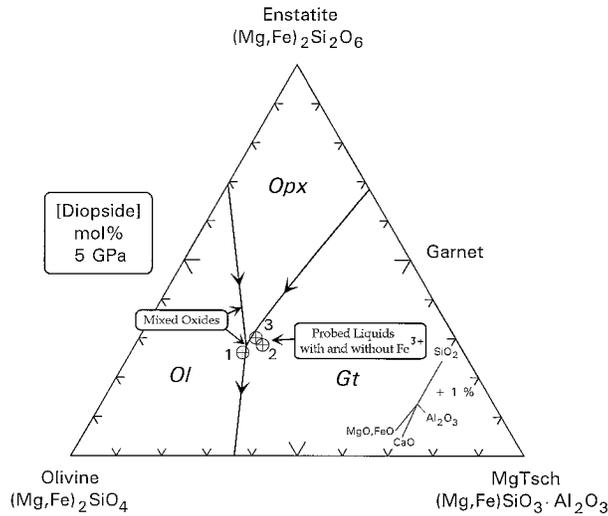
FIGURE 7. Projection of pseudoinvariant points L + Ol + Opx + Cpx + Gt from diopside ($CaMgSi_2O_6$) into the plane olivine–enstatite–magnesium Tschermak's. Bold lines are from Figure 4b, constrained from the compositions of oxide mixes. Electron probe analyses of selected experiments in Figure 4d shift the invariant point to point 1 for the liquid having all Fe as FeO (L Invpt 1; Table 2), point 2 for estimated FeO and Fe_2O_3 contents of the liquid (L Invpt 2; Table 2), point 3 for estimated FeO and Fe_2O_3 contents of the liquid projected from diopside and Fe_2O_3 (L Invpt 3; Table 2).

garnet toward point 3 in Figure 7; the pseudoinvariant point for ~11% FeO was bracketed in this way with mixes 1, 10, 15, and 17, and the liquid has the following composition: SiO_2 = 46.65(0.55), Al_2O_3 = 8.55(0.25), FeO = 11.25(0.50), MgO = 23.60(0.50), and CaO = 9.95(0.30) wt%. This is in very good agreement with the estimate given by Herzberg (1992) (Figs. 4d and 5d). Inspection of the inset in Figure 7 demonstrates that uncertainties resulting from the amount of Fe_2O_3 and how to treat it are small.

In those experiments for which 10% iron metal was added, there was an increase in the FeO contents of all phases, presumably because of the reaction of metallic iron with O that was made available from the loss of Fe to the rhenium capsule; for liquid, typical FeO contents increased from about 12 to 17%. At 1800 °C, these elevated FeO contents were established rapidly, judging from the constant 17% FeO contents in experiments that ranged in time from 5 to 60 min (Figure 2). In most cases the bulk compositions shifted into the olivine liquidus crystallization field, as seen in Figures 4c and 5c. Although we have brackets on the liquidus fields of olivine, orthopyroxene, and garnet as a second crystallizing phase, we do not have an experiment that provides a bracket on the clinopyroxene liquidus field. However, an experiment on mix 14 with both Fe⁰ and Ca added showed that clinopyroxene crystallizes at a slightly lower temperature than garnet, indicating that the CaO/Al_2O_3 ratio for this mix is similar to that for the peritectic liquid

composition. We were able to use these observations together with the compositions of the mixes in CMAS and CMFAS (~11% FeO) to estimate the following pseudoinvariant point: SiO_2 = 45.75(0.70), Al_2O_3 = 7.60(0.70), FeO = 17.00(0.75), MgO = 20.15(1.10), and CaO = 9.50(1.00) wt%.

DISCUSSION

The compositions of liquids coexisting with Ol + Opx + Cpx + Gt and containing 0–17% FeO are summarized in Table 3. The liquids in CMAS and CMFAS with 17% FeO are the bracketed compositions discussed above; the liquid in CMFAS with ~11% FeO is point 3 in Figure 7 determined by treating Fe^{3+} as a neutral component. These liquids are also shown in Figures 4e, 5e, and 8. The effect of FeO is to expand the liquidus crystallization field of garnet relative to the fields of olivine, orthopyroxene, and clinopyroxene. FeO actually depresses melting temperatures of all crystalline phases, but this effect is less for garnet than the other crystalline phases. Fe also causes a relative expansion of the crystallization fields of both orthopyroxene and clinopyroxene at the expense of olivine and an expansion in the crystallization field of clinopyroxene at the expense of orthopyroxene (Figure 6). However, inspection of the insets in Figures 4 and 5 gives a visual sense of how small these effects actually are. If only CMAS experimental data were available, it would be possible to calculate with considerable confidence the composition of a liquid in CMFAS. An example of this is given in Table 3. A liquid in equilibrium with garnet peridotite at 5 GPa in CMFAS with Fo_{90} can be calculated by simple substitution of MgO in CMAS for FeO and the exchange coefficient $K_{DFeO/MgO}^{Ol/L}$ = 0.36. The result is a liquid composition that is very similar to that which we observe experimentally, except that Al_2O_3 is too high.

The effect of FeO on expanding the garnet field at the expense of clinopyroxene slightly elevates CaO/Al_2O_3 in initial liquids (Figs. 5e and 8). Pressure estimates of komatiite multiple saturation using this parameter (Herzberg 1992, 1995) are therefore about 20% too high. However, the results reported here are in very good agreement with the more recent calibration reported by Herzberg and Zhang (1996) from melting experiments on peridotite KLB-1.

The compositions of garnets and pyroxenes that coexist with liquid at various FeO contents are given in Table 3 and shown in Figure 6; these are average compositions, which were determined from the values of K_D given above. The clinopyroxenes are subcalcic (Bertka and Holloway 1993; Longhi and Bertka 1996) and have CaO contents that range from 10% in CMAS to about 6% in CMFAS, depending on the FeO content. But we wish to emphasize that we observed substantial uncertainties in these CaO contents of clinopyroxene, typically ±1% absolute (1σ; Table 1), comparable to heterogeneities observed in garnet.

Figure 8 also illustrates that the melting of garnet pe-

TABLE 3. Summary of coexisting phase compositions (wt%) at 5 GPa

Phase	SiO_2	Al_2O_3	FeO	MgO	CaO
Liquid	48.85(0.18)	9.55(0.13)	0	30.90(0.30)	10.70(0.15)
Olivine Fo_{100}	42.43	0.21	0	57.02	0.31
Orthopyroxene	57.20	3.58	0	36.04	3.07
Clinopyroxene	55.80	3.78	0	30.62	9.49
Garnet	44.11	24.6	0	25.71	5.58
Liquid	46.65(0.55)	8.55(0.25)	11.25(0.50)	23.60(0.50)	9.95(0.30)
Olivine $Fo_{91.2}$	40.67	0.25	8.6	50.09	0.39
Orthopyroxene	56.17	3.15	5.01	32.82	2.85
Clinopyroxene	55.22	3.40	5.23	28.90	7.25
Garnet	43.29	23.96	5.14	22.46	5.15
Liquid	45.75(0.70)	7.60(0.70)	17.00(0.75)	20.15(1.10)	9.50(1.00)
Olivine $Fo_{85.4}$	39.68	0.24	13.90	45.77	0.40
Orthopyroxene	55.53	2.81	8.27	30.62	2.77
Clinopyroxene	54.69	3.07	8.80	27.45	5.99
Garnet	43.15	22.84	8.39	20.72	4.90
Liquid & Fo_{90}*	46.43	8.37	12.56	22.80	9.85
Liquid & Fo_{90}**	46.21	9.03	12.30	22.33	10.12
Liquid & Fo_{90}†	45.7	8.7	13.7	23.2	8.7
Liquid CMAS†	49.5	10.0	0	30.5	10.0
Liquid CMAS‡	49.0	9.8	0	32.2	9.0

Note: Numbers in parentheses equal 1σ.
 * Interpolated from these experimental data.
 ** Calculated from CMAS with FeO-MgO substitution.
 † Herzberg (1992).
 ‡ Fujii et al. (1989).

ridotite at 5 GPa is peritectic, consistent with previous observations (Davis and Schairer 1965; O'Hara and Yoder 1967; Herzberg et al. 1990; Herzberg 1992; Zhang and Herzberg 1994; Walter 1995; Walter et al. 1995; Kinzler 1993; Longhi 1995). At 5 GPa this peritectic in CMAS can be described by 0.12Ol + 0.70Cpx + 0.18Gt = 0.61L + 0.39Opx. In the systems CMAS and CMFAS, small uncertainties in the CaO content of clinopyroxene and in FeO-MgO partitioning can propagate to large uncertainties in the melting coefficients because of the substantial contribution of clinopyroxene to the melt.

Table 3 and Figures 4 and 5 show that liquid compo-

FIGURE 8. Projection of compositions and liquidus phase boundaries from olivine into a portion of the plane enstatite $(Mg_2Si_2O_6)$–diopside $(CaMgSi_2O_6)$-alumina (Al_2O_3), which contains both pyrope $(Mg_3Al_2Si_3O_{12})$ and grossular $(Ca_3Al_2Si_3O_{12})$. Bold lines are cotectic liquidus phase boundaries at the FeO contents shown (wt%); light lines are tie lines connecting the compositions of coexisting phases listed in Table 3.

sitions reported here in CMAS and CMFAS are in excellent agreement with previous reports (Fujii et al. 1989; Herzberg 1992). For liquid analogs of mantle peridotite containing olivine with Fo_{90}, the composition of the first drop of liquid at 5 GPa is given in Table 3, and this should be accurate to within ±0.50% (1σ). For more Fe-rich compositions, the uncertainites are elevated to about ±1.00% (Table 3). This success stems from the experimental method we adopted, wherein the composition of a liquid at an invariant point is bracketed by the liquidus phases for a wide range of bulk compositions, namely the shotgun method (e.g., Andersen 1915; O'Hara 1968; Cawthorn et al. 1973; Longhi 1987, 1995; Bertka and Holloway 1988; Herzberg 1992). This technique is particularly successful when the bulk composition is similar to a liquid composition at a cotectic or invariant point because a large pool of liquid can be created and easily analyzed; unlike experiments with low melt fractions, quench effects are minimized, and there is generally good agreement between bulk and liquid compositions that we analyzed with the electron microprobe. The shotgun technique is demonstrated to be successful at pressures that range from 1 atm to 5 GPa, and it is therefore the method of choice for ongoing multi-anvil experiments in the 10–20 GPa range.

A comparison is now made of our experimental results in CMAS at 5 GPa with the lower pressure results from the University of Texas at Dallas (Gudfinnsson and Presnall 1996). Figure 9 shows that the pressure-induced track of peritectic liquids from the Dallas laboratory decreases in normative olivine at 3.2–3.4 GPa, but this is not supported by our results. Using as a low-pressure reference frame the 3.0 GPa data of Milholland and Presnall re-
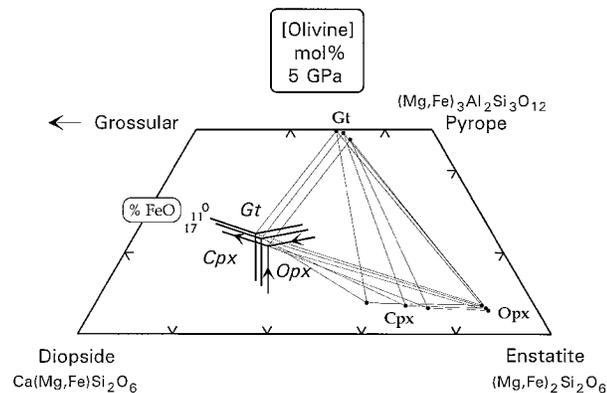
FIGURE 9. Comparison of experimental data in CMAS from this work at 5 GPa and the lower pressure determinations from the Dallas laboratory. Broken lines are pressure-induced tracks of liquids at isobaric invariant points in CMAS (L + Fo + Opx + Cpx + Gt) and in MS (L + Fo + Opx). Lines labeled 2.6 and 5 GPa are liquids coexisting with harzburgite (i.e., L + Fo + Opx). Komatiite M620 (open cross) was observed by Trønnes et al. (1992) to crystallize at 5 GPa in the following order: L, L + Ol, L + Ol + Opx, L + Ol + Opx + Gt, in excellent agreement with this work.

ported by Walter and Presnall (1994), we observed a pressure-induced peritectic liquid track that increases in normative olivine (Figure 9). Experiments on mixes with compositions at or near the Fo-En join also show that pressure increases the normative olivine content of liquids for the eutectic L + Fo + En (Figure 9), and this persists to 7 GPa (Herzberg and Zhang, unpublished data). The work of Trønnes et al. (1992) on komatiite M620 is also in excellent agreement with our experimental observations. At 5 GPa, they observed this komatiite to crystallize in the following order: L, L + Ol, L + Ol + Opx, L + Ol + Opx + Gt; this is precisely what would be predicted from our phase diagram (Figure 9). However, if the liquid at the 5 GPa invariant point contained SiO_2 that was marginally higher in content than our determination, as predicted from the results of Gudfinnsson and Presnall (1996), then orthopyroxene would not have been observed by Trønnes et al. (1992); for example, if SiO_2 in our liquids was too low by only 0.5%, the crystallization sequence for komatiite M620 would have been L, L + Ol, L + Ol + Gt, contrary to what they observed. From a thermodynamic viewpoint, the effect of pressure is to shift the composition of a liquid that is multiply saturated in the direction of the phase that has a fusion curve with the lowest slope (i.e., $\partial T/\partial P$); that phase is forsterite (Presnall and Walter 1993) rather than enstatite (Presnall and Gasparik 1990). The experimental work reported here at 5 GPa is in excellent agreement with this thermodynamic expectation and with other experimental

observations (Fujii et al. 1989; Herzberg 1992; Trønnes et al. 1992), but it is inconsistent with the work of Gudfinnsson and Presnall (1996) at 3.2–3.4 GPa.

REFERENCES CITED

Abbott, D., Burgess, L., and Longhi, J. (1994) An empirical thermal history of the Earth's upper mantle. Journal of Geophysical Research, 99, 13835–13850.

Andersen, O. (1915) The system anorthite-forsterite-silica. American Journal of Science, 4th Series, 39, 407–454.

Bertka, C.M., and Holloway, J.R. (1988) Martian mantle primary melts: An experimental study of iron-rich garnet lherzolite minimum melt composition. Proceedings of the 18th Lunar and Planetary Science Conference, 723–739.

———(1993) Pigeonite at solidus temperatures: Implications for partial melting. Journal of Geophysical Research, 98, 19755–19766.

Canil, D. (1992) Orthopyroxene stability along the peridotite solidus and the origin ofcratonic lithosphere beneath southern Africa. Earth and Planetary Science Letters, 111, 83–95.

Cawthorn, R.G. (1975) Degrees of melting in mantle diapirs and the origin of ultrabasic liquids. Earth and Planetary Science Letters, 27, 113–120.

Cawthorn, R.G., Ford, C.E., Biggar, G.M., Bravo, M.S., and Clarke, D.B. (1973) Determination of the liquid composition in experimental samples: Discrepancies between microprobe analyses and other methods. Earth and Planetary Science Letters, 21, 1–5.

Chen, C.-H., and Presnall, D.C. (1975) The system Mg_2SiO_4-SiO_2 at pressures up to 25 kilobars. American Mineralogist, 60, 398–406.

Davis, B.T.C., and Schairer, J.F. (1965) Melting relations in the join diopside-forsterite-pyrope at 40 kilobars and at one atmosphere. Carnegie Institution of Washington, Yearbook, 64, 123–126.

Fujii, T., Tachikara, M., and Kurita, K. (1989) Melting experiments in the system CaO-MgO-Al_2O_3-SiO_2 to 8 GPa: Constraints to the origin of komatiites. Transactions of the American Geophysical Union, 70, 483.

Gudfinnsson, G.H., and Presnall, D.C. (1997) Melting relations of model lherzolite in the system CaO-MgO-Al_2O_3-SiO_2 at 2.4 to 3.4 GPa and the generation of komatiites. Journal of Geophysical Research 101, 27,701–27,709.

Herzberg, C.T. (1992) Depth and degree of melting of komatiites. Journal of Geophysical Research, 97, 4521–4540.

———(1995) Generation of plume magmas through time: An experimental perspective. Chemical Geology, 126, 1–16.

Herzberg, C., Gasparik, T., and Sawamoto, H. (1990) Origin of mantle peridotite: Constraints from melting experiments to 16.5 GPa. Journal of Geophysical Research, 95, 15779–15803.

Herzberg, C.T., and Zhang, J. (1996) Melting experiments on anhydrous peridotite KLB-1: Compositions of magmas in the upper mantle and transition zone. Journal of Geophysical Research, 101, 8271–8295.

Ito, E., and Takahashi, E. (1987) Melting of peridotite under the lower mantle condition. Nature, 328, 514–517.

Kinzler, R.J. (1993) Mantle melting processes at the spinel-garnet transition (17–21 kb). Transactions of the American Geophysical Union, 73, 316.

Lahaye, Y., Arndt, A., Byerly, G., Chauvel, C., Fourcade, S., and Gruau, G. (1995) The influence of alteration on the trace-element and Nd isotopic compositions of komatiites. Chemical Geology, 126, 43–64.

Longhi, J. (1987) Liquidus equilibria and solid solution in the system $CaAl_2Si_2O_8$-Mg_2SiO_4-$CaSiO_3$-SiO_2 at low pressure. American Journal of Science, 287, 265–331.

———(1995) Liquidus equilibria of some primary lunar and terrestrial

melts in the garnet stability field. Geochimica et Cosmochimica Acta, 59, 2375–2386.

Longhi, J., and Bertka, C.M. (1996) Graphical analysis of pigeonite-augite liquidus equilibria. American Mineralogist, 81, 685–695.

McFarlane, E.A., Drake, M.J., and Rubie, D. (1994) Element partitioning between Mg-perovskite, magnesiowustite, and silicate melt at conditions of the Earth's mantle. Geochimica et Cosmochimica Acta, 58, 5161–5172.

Nisbet, E.G., Cheadle, M.J., Arndt, N.T., and Bickle, M.J. (1993) Constraining the potential temperature of the Archaean mantle: A review of the evidence from komatiites. Lithos, 30, 291–307.

O'Hara, M.J. (1968) The bearing of phase equilibria studies in synthetic and natural systems on the origin of basic and ultrabasic igneous rocks. Earth Science Reviews, 4, 69–133.

O'Hara, M.J., and Yoder, H.S., Jr. (1967) Formation and fractionation of basic magmas at high pressures. Scottish Journal of Geology, 3, 67–117.

Presnall, D.C., and Gasparik, T. (1990) Melting of enstatite from 10 to 16.5 GPa, the beta phase-majorite eutectic at 16.5 GPa, and implications for the origin of the mantle. Journal of Geophysical Research, 95, 15771–15777.

Presnall, D.C., and Walter, M.J. (1993) Melting behavior of forsterite, Mg_2SiO_4, from 9.7 to 16.5 GPa. Journal of Geophysical Research, 98, 19777–19783.

Steinbach, V., and Yuen, D.A. (1994) Melting instabilities in the transition zone. Earth and Planetary Science Letters, 127, 67–75.

Takahashi, E. (1986) Melting of a dry peridotite KLB-1 up to 14 GPa: Implications on the origin of peridotitic upper mantle. Journal of Geophysical Research, 91, 9367–9382.

Takahashi, E., and Scarfe, C.M. (1985) Melting of a peridotite at > 15 GPa and the genesis of komatiite. Nature, 315, 566–568.

Trønnes, R.G., Canil, D., and Wei, K. (1992) Element partitioning between silicate minerals and coexisting melts at pressures of 1–17 GPa, and implications for mantle evolution. Earth and Planetary Science Letters, 111, 241–255.

Walker, D., and Agee, C. (1989) Partitioning ''equilibrium'', temperature gradients, and constraints on Earth differentiation. Earth and Planetary Science Letters, 96, 49–60.

Walter, M.J. (1993) Thermally-induced chemical diffusion in melting experiments at high pressure. Transactions of the American Geophysical Union, 74, 350.

———(1995) Melting reactions of fertile garnet peridotite. Transactions of the   merican Geophysical Union, 76, S297.

Walter, M.J., and Presnall, D.C. (1994) Melting behavior of simplified lherzolite in the system $CaO-MgO-Al_2O_3-SiO_2-Na_2O$ from 7 to 35 kbar. Journal of Petrology, 35, 329–359.

Walter, M.J., Sisson, T.W., and Presnall, D.C. (1995) A mass proportion method for calculating melting reactions and application to melting of model upper mantle lherzolite. Earth and Planetary Science Letters, 135, 77–90.

Wei, K., Trønnes, R.G., and Scarfe, C.M. (1990) Phase relations of aluminum-undepleted and aluminum-depleted komatiites at pressures of 4 to 12 GPa. Journal of Geophysical Research, 95, 15817–15828.

Xie, Q., Kerrich, R., and Fan, J. (1993) HFSE/REE fractionations recorded in three komatiite-basalt sequences, Archean Abitibi greenstone belt: Implications for multiple plume sources and depths. Geochimica et Cosmochimica Acta, 57, 4111–4118.

Zhang, J., and Herzberg, C. (1994) Melting experiments on anhydrous peridotite KLB-1 from 5.0 to 22.5 GPa. Journal of Geophysical Research, 99, 17729–17742.